Appl Compos Mater (2011) 18:385–396
DOI 10.1007/s10443-010-9163-x

Effects of Steam Environment on Fatigue Behavior of Two SiC/[SiC+Si_3N_4] Ceramic Composites at 1300°C

Marina B. Ruggles-Wrenn · Vipul Sharma

Received: 20 May 2010 / Accepted: 4 August 2010 / Published online: 1 September 2010
© US Government 2010

Abstract The fatigue behaviors of two SiC/[SiC+Si_3N_4] ceramic matrix composites (CMC) were investigated at 1,300°C in laboratory air and in steam. Composites consisted of a crystalline [SiC+Si_3N_4] matrix reinforced with either Sylramic™ or Sylramic-iBN fibers (treated Sylramic™ fibers that possess an in situ BN coating) woven in a five-harness satin weave fabric and coated with a proprietary boron-containing dual-layer interphase. The tensile stress–strain behaviors were investigated and the tensile properties measured at 1,300°C. Tension–tension fatigue behaviors of both CMCs were studied for fatigue stresses ranging from 100 to 180 MPa. The fatigue limit (based on a run-out condition of 2×10^5 cycles) in both air and steam was 100 MPa for the CMC containing Sylramic™ fibers and 140 MPa for the CMC reinforced with Sylramic-iBN fibers. At higher fatigue stresses, the presence of steam caused noticeable degradation in fatigue performance of both composites. The retained strength and modulus of all run-out specimens were characterized. The materials tested in air retained 100% of their tensile strength, while the materials tested in steam retained only about 90% of their tensile strength.

Keywords Ceramic-matrix composites (CMCs) · Fatigue · High-temperature properties · Fractography

1 Introduction

Advances in power generation systems for aircraft engines, land-based turbines, rockets, and, most recently, hypersonic missiles and flight vehicles have raised the demand for

The views expressed are those of the authors and do not reflect the official policy or position of the United States Air Force, Department of Defense or the U. S. Government.

This material was provided to the Air Force Institute of Technology by the Air Force Research Laboratory, WPAFB

M. B. Ruggles-Wrenn (✉) · V. Sharma
Department of Aeronautics and Astronautics, Air Force Institute of Technology,
Wright-Patterson Air Force Base, OH 45433-7765, USA
e-mail: marina.ruggles-wrenn@afit.edu

structural materials that have superior long-term mechanical properties under high temperature, high pressure, and varying environmental factors, such as moisture. Because of their low density, high strength and fracture toughness at high temperatures silicon carbide fiber-reinforced silicon-carbide matrix composites are currently being evaluated for aircraft engine hot-section components [1–4]. In these applications the composites will be subjected to sustained and cyclic loadings at elevated temperatures in oxidizing environments. Therefore a thorough understanding of high-temperature mechanical behavior and performance of SiC/SiC composites in service environments is critical to design with and life prediction for these materials.

The main advantage of CMCs over monolithic ceramics is their superior toughness, tolerance to the presence of cracks and defects, and non-catastrophic mode of failure. This key advantage is achieved though a proper design of a fiber/matrix interphase, which serves to deflect matrix cracks and to prevent early failure of the fibrous reinforcement [5–9]. The most significant problem hindering SiC-fiber-containing CMCs is oxidation embrittlement [10]. Typically the embrittlement occurs once oxygen enters through the matrix cracks and reacts with the fibers and the fiber coatings [11–13]. The degradation of fibers and fiber coatings is typically accelerated by the presence of moisture [14–16]. Composite degradation may be further accelerated by cyclic loading, as the reaction gases are expelled from matrix cracks during unloading and oxidizing environment is drawn into the composite through the matrix cracks during reloading [10].

Several recent studies evaluated mechanical behavior of high-performance SiC/SiC CMCs at elevated temperature. Morscher et al. [17] studied creep at 1,315°C in air of the composites consisting of high modulus SiC fibers (Hi-Nicalon S) and a melt-infiltrated SiC matrix. Ojard et al. [18, 19] and Morscher et al. [4] reported on the elevated-temperature mechanical performance of a ceramic composite, consisting of a melt-infiltrated SiC matrix reinforced with Sylramic-iBN SiC fibers, a CMC system developed at NASA Glenn Research Center [20]. The present paper aims to evaluate the fatigue behavior of two high-performance polycrystalline SiC fiber-reinforced ceramic composites, which are made by polymer infiltration and pyrolysis (PIP) method. Polymer infiltration and pyrolysis is an attractive processing approach because of its relatively low cost. In addition, this processing method allows near-net-shape molding and fabrication, resulting in nearly fully dense composites [21–23]. The materials studied in this effort are reinforced with Sylramic™ and Sylramic-iBN fibers. Fatigue tests were conducted at 1,300°C in air and steam environments for stress levels ranging from 100 to 180 MPa. Resulting fatigue performance imposes limitations on the use of these materials in high-temperature applications.

2 Material and Experimental Arrangements

The materials studied were two SiC fiber-reinforced composites with a PIP-derived crystalline [SiC+Si_3N_4] matrix manufactured by COI Ceramics, Inc. (San Diego, CA). The first composite (Syl/[SiC+Si_3N_4]) was reinforced with Sylramic™ fibers, while the second composite (Syl-iBN/[SiC+Si_3N_4]) contained Sylramic-iBN, i.e. treated Sylramic™ fibers that possess an in situ BN coating. In processing of both composites, the woven five-harness satin weave (5HSW) fiber cloth was coated with a proprietary boron-containing dual-layer interphase, stacked and infiltrated with a mixture of polymer, filler particles and solvent. In the case of the Syl-iBN/ [SiC+Si_3N_4] composite, additional filler designed to inhibit oxidation was also introduced. During pyrolysis at temperatures >1,000°C, the polymer was pyrolyzed to a crystalline [SiC+Si_3N_4] matrix. The infiltration and pyrolysis

procedure was repeated several times to increase the density of the matrix. Both composites were comprised of 12 plies of woven fabric in a 0°/90° layup, with a finished fiber volume of approximately 42% and an open porosity of ~3%.

A servocontrolled MTS mechanical testing machine equipped with hydraulic water-cooled wedge grips, a compact two-zone resistance-heated furnace, and two temperature controllers was used in all tests. An MTS TestStar II digital controller was employed for input signal generation and data acquisition. Strain measurement was accomplished with an MTS high-temperature air-cooled uniaxial extensometer of 12.5-mm gage length. Tests in steam environment employed an alumina susceptor (tube with end caps), which fits inside the furnace. The specimen gage section is located inside the susceptor, with the ends of the specimen passing through slots in the susceptor. Steam is introduced into the susceptor (through a feeding tube) in a continuous stream with a slightly positive pressure, expelling the dry air and creating a near 100% steam environment inside the susceptor. For elevated temperature testing, thermocouples were bonded to the specimen using alumina cement (Zircar) to calibrate the furnace on a periodic basis. The furnace controllers (using non-contacting thermocouples exposed to the ambient environment near the test specimen) were adjusted to determine the settings needed to achieve the desired temperature of the test specimen. The determined settings were then used in actual tests. The power settings for testing in steam were determined by placing the specimen instrumented with thermocouples in steam environment and repeating the furnace calibration procedure. Fracture surfaces of failed specimens were examined using SEM (FEI Quanta 200 HV) as well as an optical microscope (Zeiss Discovery V12).

All tests were performed at 1,300°C. Dog bone shaped specimens of 152 mm total length with an 8-mm-wide gage section were used in all tests. In all tests, a specimen was heated to test temperature at 1°C/min, and held at temperature for additional 25 min prior to testing. In air, tensile tests were performed in stroke control with a constant displacement rate of 0.05 mm/s. Tension–tension fatigue tests were conducted in load control with an R ratio (minimum to maximum stress) of 0.05 at a frequency of 1.0 Hz. Fatigue run-out was set to 2×10^5 cycles. The 2×10^5 cycle count represents the number of loading cycles expected in aerospace applications at that temperature. Fatigue run-out limits were defined as the highest stress level, for which run-out was achieved. Cyclic stress–strain data were recorded throughout each test. Thus stiffness degradation as well as strain accumulation with fatigue cycles and/or time could be examined. All specimens that achieved run-out were subjected to tensile test to failure at 1,300°C in laboratory air to determine the retained strength and stiffness. It is worthy of note that in all tests reported below, the failure occurred within the gage section of the extensometer.

3 Results and Discussion

3.1 Monotonic Tension

Tensile stress–strain behavior of the two composites at 1,300°C is typified in Fig. 1. For Syl/[SiC+Si_3N_4], the average ultimate tensile strength (UTS) was 188 MPa, elastic modulus, 129 GPa, and failure strain, 0.16%. For Syl-iBN/[SiC+Si_3N_4], the average UTS was 241 MPa, elastic modulus, 147 GPa, and failure strain 0.25%. The Syl-iBN/[SiC+Si_3N_4] composite displayed an ultimate strength advantage of ~53 MPa over the Syl-iBN/[SiC+Si_3N_4] CMC. This is attributed primarily to the in situ BN coating that protects the fibers from detrimental environmental effects introduced during processing [24]. The average proportional limit for Syl-iBN/[SiC+Si_3N_4] was determined to be a high 144 MPa. The stress–strain curve obtained for Syl-iBN/[SiC+Si_3N_4] exhibits a nearly bilinear behavior typical of a brittle

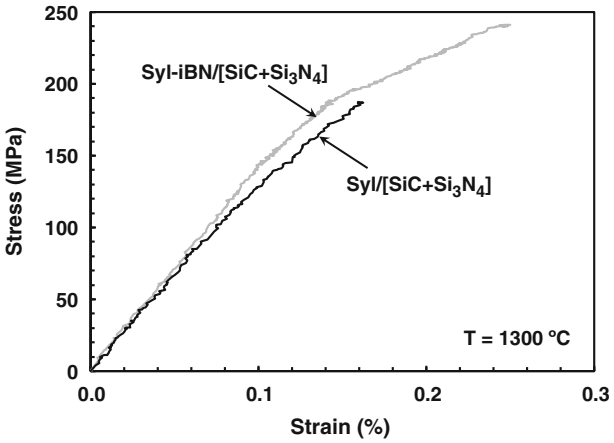

Fig. 1 Tensile stress–strain curves obtained for Syl/[SiC+Si_3N_4] and Syl-iBN/[SiC+Si_3N_4] ceramic composites at 1,300°C in laboratory air

ceramic composite. The stress–strain behavior is linear up to the proportional limit, where nonlinear behavior caused by matrix cracking occurs. Afterwards, the stress–strain curve continues with a decreased slope. Conversely, the stress–strain curve obtained for Syl/[SiC+Si_3N_4] at 1,300°C is nearly linear to failure and does not exhibit a clear proportional limit.

3.2 Tension–Tension Fatigue

Results of the tension–tension fatigue tests are summarized in Table 1. Figure 2 shows stress vs cycles to failure (S–N) curves for both composites. For Syl/[SiC+Si_3N_4] the fatigue limit was 100 MPa (53%UTS) at 1,300°C in air and in steam. For Syl-iBN/[SiC+Si_3N_4] the fatigue limit was 160 MPa (66%UTS) in air and 140 MPa (58%UTS) in steam. Presence of steam noticeably degrades fatigue performance of both composites at higher fatigue stress

Table 1 Summary of fatigue results for Syl/[SiC+Si_3N_4] and Syl-iBN/[SiC+Si_3N_4] ceramic composites at 1,300°C in laboratory air and steam environments

Test environment	Max stress (MPa)	Cycles to failure	Failure strain (%)
Syl/[SiC+Si_3N_4]			
Laboratory air	100	200,000[a]	0.055
Laboratory air	120	28,515	0.027
Laboratory air	140	10,104	0.036
Steam	100	200,000[a]	0.088
Steam	120	14,688	0.054
Steam	140	2,329	0.060
Syl-iBN/[SiC+Si_3N_4]			
Laboratory air	140	200,000[a]	0.073
Laboratory air	160	200,000[a]	0.080
Laboratory air	180	22,808	0.072
Steam	140	200,000[a]	0.101
Steam	160	153,143	0.106
Steam	180	5,765	0.098

[a] Run-out, failure of specimen did not occur when the test was terminated

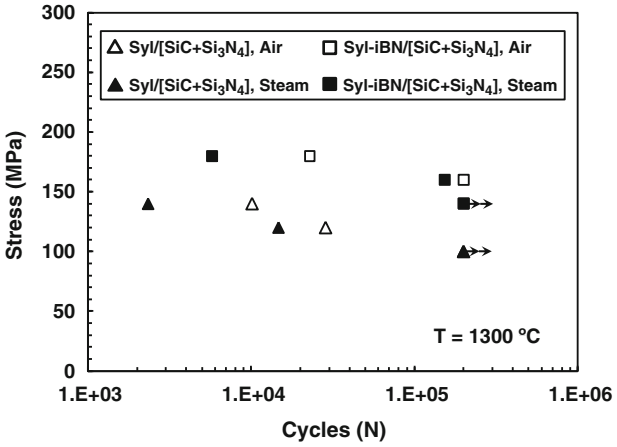

Fig. 2 Fatigue S–N curves for Syl/[SiC+Si_3N_4] and Syl-iBN/[SiC+Si_3N_4] ceramic composites at 1,300°C in air and in steam. *Arrow* indicates that failure of specimen did not occur when the test was terminated

levels. For Syl/[SiC+Si_3N_4], the reduction in fatigue life due to steam was 48% at the fatigue stress of 120 MPa and 77% at the fatigue stress of 140 MPa. For Syl-iBN/[SiC+Si_3N_4], the loss of fatigue life due to steam was 23% at the fatigue stress of 160 MPa and 75% at the fatigue stress of 180 MPa.

Maximum and minimum strains as functions of cycle number obtained at 1,300°C in air and in steam are presented in Fig. 3 (a) and (b) for Syl/[SiC+Si_3N_4] and Syl-iBN/[SiC+Si_3N_4], respectively. It is seen that ratcheting (progressive strain accumulation with cycles) takes place in all fatigue tests conducted in this study. For both composites, ratcheting develops gradually, and is more noticeable in the latter part of the fatigue tests. Earlier onset of ratcheting is observed in tests with higher fatigue stress levels. Results in Fig. 3 reveal that the Syl-iBN/[SiC+Si_3N_4] produced larger maximum strains during fatigue cycling than the Syl/[SiC+Si_3N_4]. At 1,300°C in air, maximum strains produced by Syl/[SiC+Si_3N_4] ranged from 0.14% to 0.16%, while those produced by Syl-iBN/[SiC+Si_3N_4] ranged from 0.19% to 0.21%. As seen in Fig. 3, both composites generated somewhat larger strains in steam than in air. At 1,300°C in steam, maximum strains reached 0.17% for Syl/[SiC+Si_3N_4] and 0.22% for Syl-iBN/[SiC+Si_3N_4].

Of interest is the reduction in modulus (hysteresis modulus determined from the maximum and minimum stress–strain data points during a load cycle), reflecting the damage development during fatigue cycling. Figure 4 shows change in normalized modulus (i.e. modulus normalized by the modulus obtained on the first cycle) with fatigue cycles. It is noteworthy that although some tests achieved run-out a small decrease in normalized modulus with cycling was still observed. This drop in modulus is hypothesized to be due to a low level of microcracking. As seen in Fig. 4, modulus loss increased with increasing fatigue stress for both composites. Continuous drop in modulus observed at higher fatigue stress levels suggests progressive damage accumulation with continued cycling. Furthermore, decrease in normalized modulus becomes more pronounced in steam environment for both CMCs. In the case of Syl/[SiC+Si_3N_4], the normalized modulus loss was limited to 15% in air and to 22% in steam. In the case of Syl-iBN/[SiC+Si_3N_4], the decrease in normalized modulus reached 25% in air and 33% in steam. This suggests accelerated damage growth in steam. The damage development in these composites is likely to proceed by the oxidation-induced growth of matrix cracks. Progressive matrix cracking exposes fibers to oxidizing environment and thus accelerates intrinsic fiber degradation. Moreover, once oxygen enters the matrix cracks, BN and SiC react to form gaseous species and solid

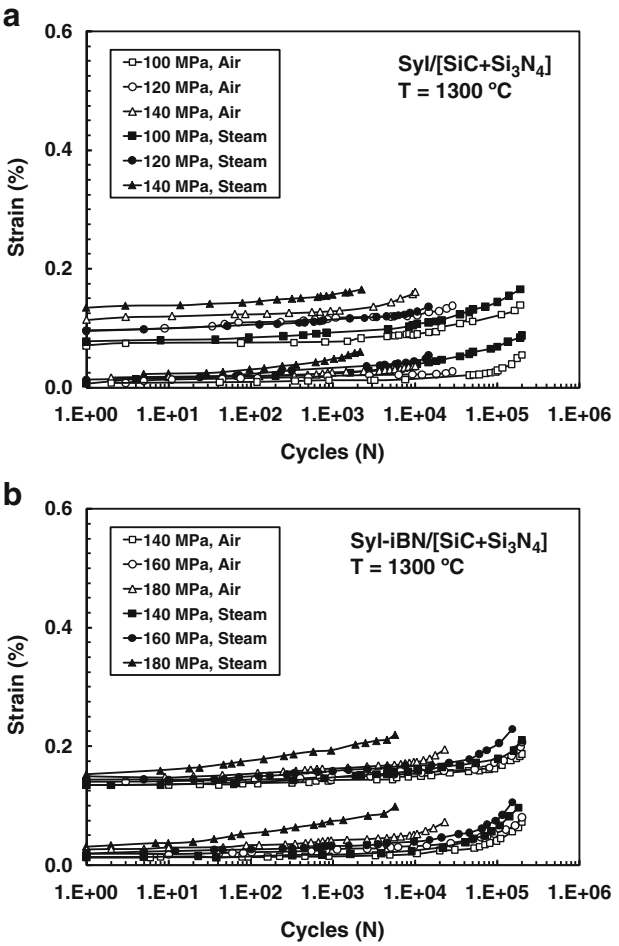

Fig. 3 Maximum and minimum strains as functions of cycle number at 1,300°C in air and in steam for: **a** Syl/[SiC+Si_3N_4] and **b** Syl-iBN/[SiC+Si_3N_4] ceramic composites

borosilicate reaction products that bond exposed fibers together [4], causing fiber failures due to local stress concentration from load sharing created by strongly fused fibers.

Retained strength and stiffness of the fatigue specimens that achieved run-out are summarized in Table 2. Evaluation of retained properties is useful in assessing the damage state of the composite subjected to prior loading. It is seen that specimens of both composites subjected to prior fatigue in air exhibited no loss of tensile strength, irrespective of the fatigue stress level. However, modulus loss of 5–6% was observed for both CMCs. In contrast, prior fatigue in steam caused reduction in both strength and stiffness of the two composites. Strength loss in steam was ~10% for both materials. Modulus loss in steam was 7% for Syl/[SiC+Si_3N_4] and 12% for Syl-iBN/[SiC+Si_3N_4].

3.3 Composite Microstructure

All specimens tested in this study were examined with optical and scanning electron microscopes to elucidate failure and damage mechanisms. Optical micrographs of fractured Syl/[SiC+Si_3N_4] and Syl-iBN/[SiC+Si_3N_4] specimens are shown in Fig. 5 (a) and (b), respectively. The fracture surfaces in Fig. 5 are similar in appearance, both are relatively flat

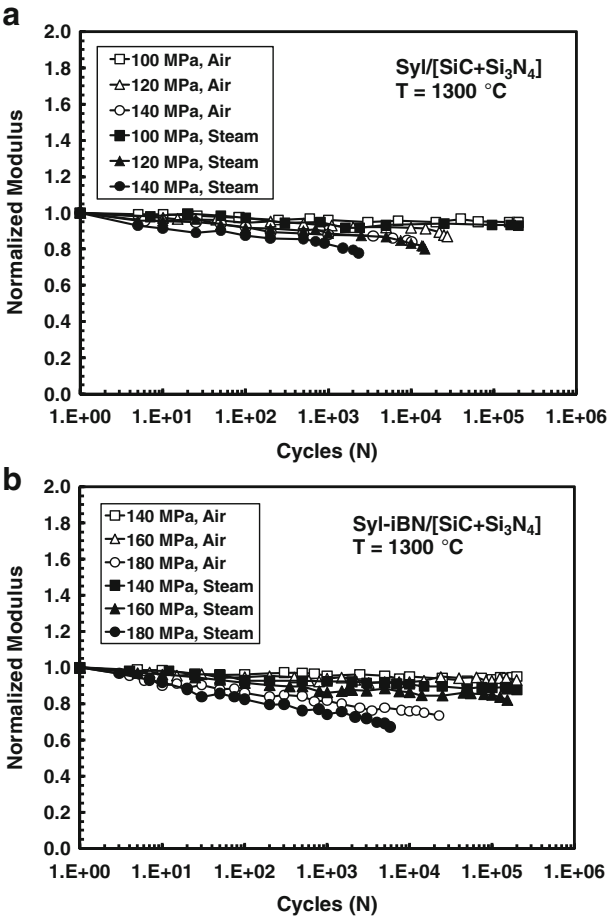

Fig. 4 Normalized modulus vs fatigue cycles at 1,300°C in air and in steam for: **a** Syl/[SiC+Si_3N_4] and **b** Syl-iBN/[SiC+Si_3N_4] ceramic composites

and perpendicular to the loading direction. Note that the fracture surfaces in Fig. 5 are typical and representative of all optical micrographs obtained in this study. Furthermore, no distinctive features attributable to test type (monotonic tension vs fatigue) or test environment (air vs steam) could be discerned at the low magnification such as that of Fig. 5. Therefore for the sake of brevity optical micrographs of other fractured specimens are not shown.

The SEM micrographs of the fracture surfaces of the Syl/[SiC+Si_3N_4] specimens tested in fatigue at 1,300°C in air and in steam are shown in Figs. 6 and 7, respectively. All images obtained at lower magnification in air (Figs. 6(a) and 6(d)) and in steam (Figs. 7(a) and 7(d)) show very similar nearly planar fracture surfaces. Yet the specimen in Fig. 6(a) achieved fatigue run-out in air and was failed in a subsequent tension test, while the specimen in Fig. 7(d) failed after only 2,329 fatigue cycles in steam. The influence of test environment becomes noticeable in images obtained at intermediate magnification. The SEM micrographs of specimens tested in air (Figs. 6(b) and 6(e)) show fracture along different planes, fiber debonding and pullout of fiber bundles. In contrast, the fracture surfaces of the specimens tested in steam (Figs. 7(b) and 7(e)) show fracture surfaces that are almost completely planar. The degrading effects of steam environment as well as those of higher fatigue stress level are clearly revealed in higher magnification images. Consider the

Table 2 Retained properties of the Syl/[SiC+Si_3N_4] and Syl-iBN/[SiC+Si_3N_4] specimens subjected to prior fatigue in laboratory air and in steam environment at 1,300°C. Retained properties measured at 1,300°C in laboratory air

Fatigue stress (MPa)	Fatigue environment	Retained strength (MPa)	Strength retention (%)	Retained modulus (GPa)	Modulus retention (%)	Strain at failure (%)
Syl/[SiC+Si_3N_4]						
100	Air	206	≥100	122	95	0.20
100	Steam	171	91	120	93	0.15
Syl-iBN/[SiC+Si_3N_4]						
140	Air	246	≥100	140	95	0.27
160	Air	247	≥100	137	94	0.29
140	Steam	215	89	129	88	0.23

specimen in Fig. 6 (c) that achieved run-out with σ_{max}=100 MPa in air. Its fibers, fiber coating, and matrix show little or no physical degradation. In contrast the matrix of the specimen subjected to fatigue in air with σ_{max}=140 MPa (Fig. 6 (f)) appears to be severely damaged, although its fibers and fiber coating remain relatively intact. Similar observation can be made regarding the specimen that achieved run-out with σ_{max}=100 MPa in steam (Fig. 7 (c)). While its fibers and fiber coating appear undamaged, the matrix between the fibers has disintegrated in places. Severest degradation is seen in the case of specimen tested in steam with σ_{max}=140 MPa (Fig. 7 (e)), which also produced the shortest fatigue life of 2,329 cycles. The fibers are severely damaged, the fiber coating is absent, and matrix appears to have disintegrated.

Figures 8 and 9 show the fracture surfaces of the Syl-iBN/[SiC+Si_3N_4] specimens tested in fatigue at 1,300°C in air and in steam, respectively. Notably the SEM micrographs obtained at low magnification in air (Figs. 8(a) and 8(d)) and in steam (Figs. 9(a) and 9(d)) are alike. All show the nearly planar fracture surfaces. Furthermore the fracture surfaces in Figs. 8(a) and 8(d) and Figs. 9(a) and 9(d) differ little from the low magnification images obtained for the Syl/[SiC+Si_3N_4] composite. The same can be said about the images obtained at intermediate magnification (Figs. 8(b) and 8(e)) and (Figs. 9(b) and 9(e)). At this magnification the characteristics observed in the Syl-iBN/[SiC+Si_3N_4] fracture surfaces are akin to those seen in the Syl/[SiC+Si_3N_4] fracture surfaces in Figs. 6(b) and 6(e) and

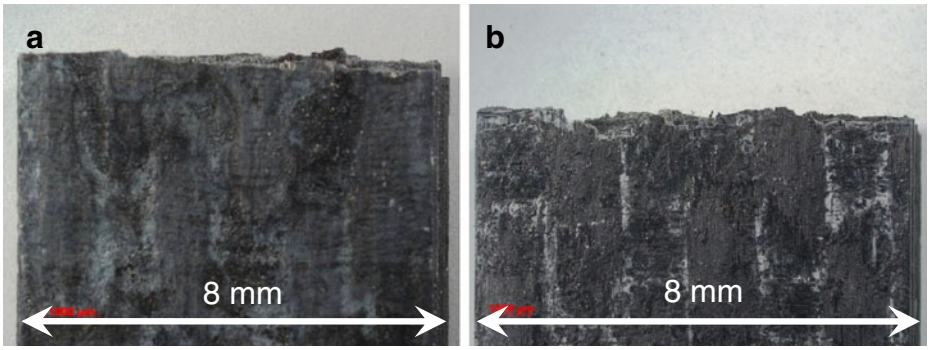

Fig. 5 Fracture surfaces obtained in fatigue tests conducted at 1,300°C in air: **a** Syl/[SiC+Si_3N_4], σ_{max}= 140 MPa and **b** Syl-iBN/[SiC+Si_3N_4], σ_{max}=140 MPa

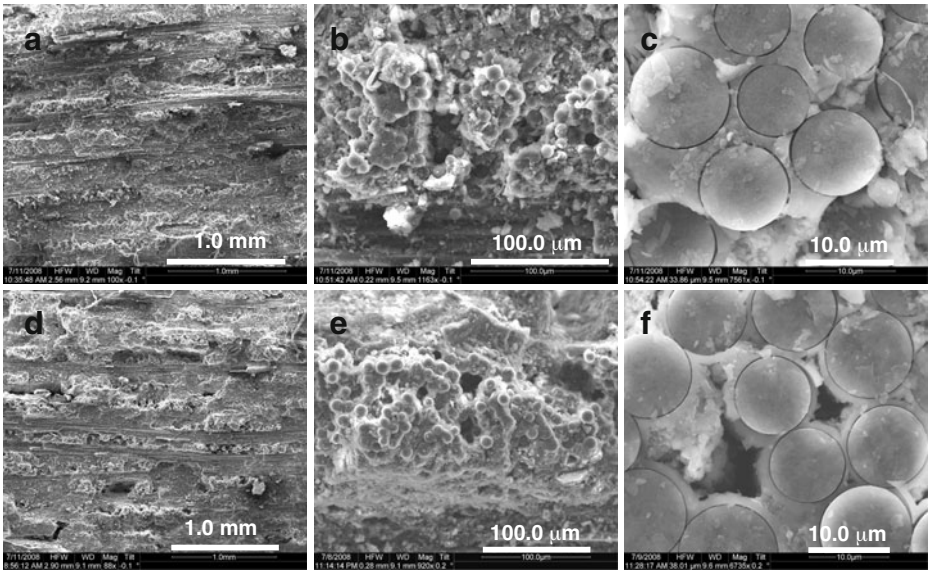

Fig. 6 SEM micrographs of fracture surfaces of Syl/[SiC+Si_3N_4] specimens tested in fatigue at 1,300°C in air: (**a**–**c**) with σ_{max}=100 MPa and (**d**–**f**) with σ_{max}=140 MPa

Figs. 7(b) and 7(e). Higher magnification images in Figs. 8(c) and 8(f) and Figs. 9(c) and 9(f) are of more interest. Fracture surface of the Syl-iBN/[SiC+Si_3N_4] specimen that achieved fatigue run-out at 140 MPa in air (Fig. 8 (c)) reveals some damage to the matrix and degradation of the interphase (arrow). However, fibers appear to be undamaged. The fracture surface in Fig. 8 (f) of the specimen that failed after 22,808 cycles with σ_{max}=140 MPa in

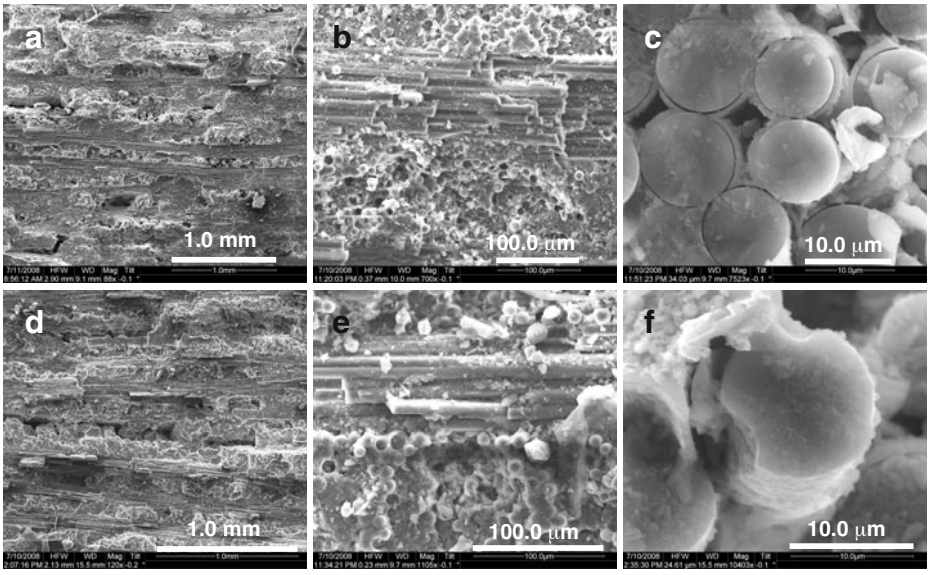

Fig. 7 SEM micrographs of fracture surfaces of Syl/[SiC+Si_3N_4] specimens tested in fatigue at 1,300°C in steam: (**a**–**c**) with σ_{max}=100 MPa and (**d**–**f**) with σ_{max}=140 MPa

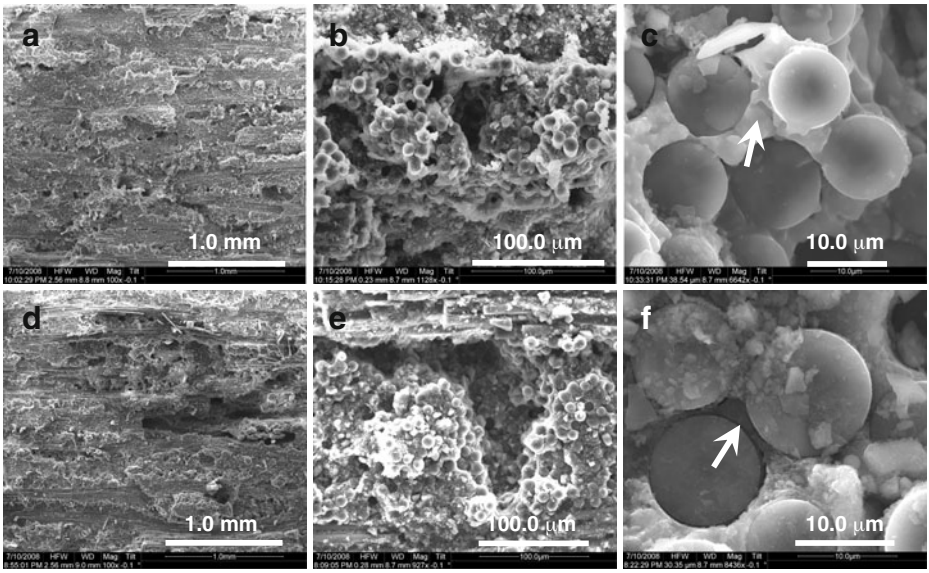

Fig. 8 SEM micrographs of fracture surfaces of Syl-iBN/[SiC+Si_3N_4] specimens tested in fatigue at 1,300°C in air: (**a**–**c**) with σ_{max}=140 MPa and (**d**–**f**) with σ_{max}=180 MPa

air also shows damage to the interphase (arrow), while the fibers remain intact. The damage to the interphase becomes more pronounced in steam, especially in tests of longer duration. Figure 9 (c) shows the fracture surface of the specimen that achieved run-out with σ_{max}= 140 MPa in steam. Interphase material is severely degraded, matrix oxidation is also evident. Yet individual fibers still appear to be physically intact. The fracture surface of the specimen

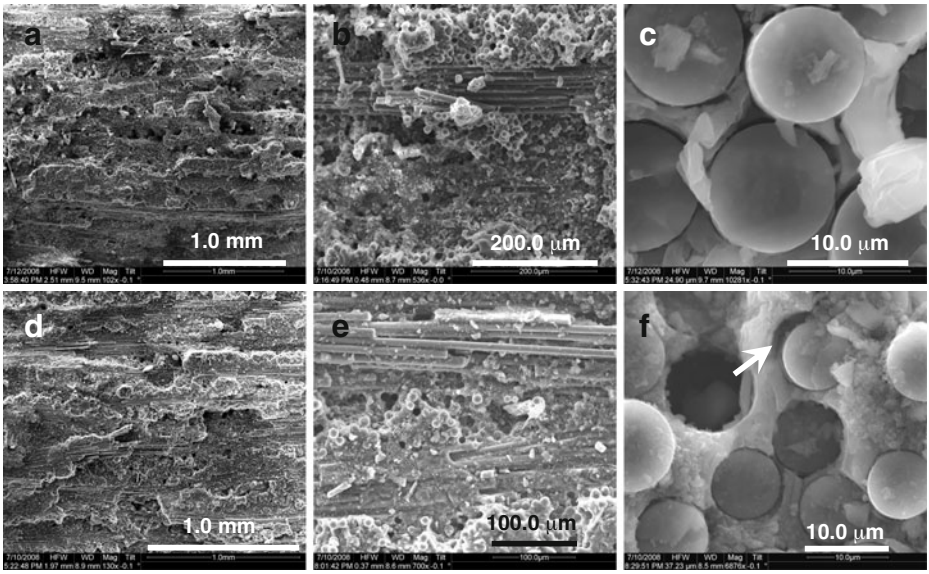

Fig. 9 SEM micrographs of fracture surfaces of Syl-iBN/[SiC+Si_3N_4] specimens tested in fatigue at 1,300°C in steam: (**a**–**c**) with σ_{max}=140 MPa and (**d**–**f**) with σ_{max}=180 MPa

fatigued with σ_{max}=180 MPa in steam (Fig. 9 (e)) also shows degradation of the interphase (arrow) as well as matrix oxidation. Once again, the fibers do not appear to have suffered significant damage. It is possible that the in situ grown BN layer provided an oxidation resistant physical barrier that delayed fiber damage whenever the fiber tows were exposed to oxidizing environment during matrix cracking.

4 Concluding Remarks

The tensile stress–strain behaviors of the Syl/[SiC+Si_3N_4] and Syl-iBN/[SiC+Si_3N_4] composites were investigated and the tensile properties measured at 1,300°C. The UTS of the Syl-iBN/[SiC+Si_3N_4] composite was ~28% higher than that of the Syl/[SiC+Si_3N_4] composite. This improvement in ultimate tensile strength is attributed to the in situ BN coating that protects fibers from environmental degradation during processing.

Tension–tension fatigue behavior of both composites was studied at 1,300°C in air and in steam. Fatigue stress levels ranged from 100 to 140 MPa for the Syl/[SiC+Si_3N_4] composite and from 140 to 180 MPa for the Syl-iBN/[SiC+Si_3N_4] composite. Of the two materials studied the Syl-iBN/[SiC+Si_3N_4] composite exhibits a considerably better fatigue performance at 1,300°C in both air and steam environments. The fatigue limit of the Syl/[SiC+Si_3N_4] composite is 100 MPa (53%UTS) in both air and steam. The fatigue limit of the Syl-iBN/[SiC+Si_3N_4] CMC is 160 MPa (66%UTS) in air and 140 MPa (58%UTS) in steam. The presence of steam degrades fatigue performance of both materials at higher fatigue stress levels. The detrimental effects of steam on fatigue life of the Syl/[SiC+Si_3N_4] composite become noticeable as the fatigue stresses exceed 64%UTS. For Syl-iBN/[SiC+Si_3N_4] the damaging effects of steam become significant when the fatigue stresses exceeds 67%UTS.

Both composites retain 100% of their tensile strength after achieving fatigue run-out at 1,300°C in air. However, modulus loss of 5–6% is observed for both materials. Following fatigue run-out in steam both materials retain only ~90% of their tensile strength. Modulus loss is limited to 7% for Syl/[SiC+Si_3N_4] and to 12% for Syl-iBN/[SiC+Si_3N_4].

Acknowledgement The authors would like to thank Dr. G. Fair for many valuable discussions. The financial support of the Air Force Research Laboratory Materials and Manufacturing Directorate (Dr. M. Cinibulk) is highly appreciated.

References

1. Brewer, D.: HSR/EPM combustor materials development program. Mater. Sci. Eng. A. **A261**, 284–291 (1999)
2. Brewer, D., Ojard, F., Gibler, M.: Ceramic matrix composite combustor liner rig test. ASME Turbo Expo 2000, Munich Germany, May 8–11, 2000, ASME Paper 2000-GT-0670.
3. Corman, G.S., Luthra, K.: Silicon melt infiltrated ceramic composites (HiPerComp). In: Bansal, N. (ed.) Hand book of ceramic composites, pp. 99–115. Kluwer, NY (2005)
4. Morscher, G.N., Ojard, G., Miller, R., Gowayed, Y., Santhosh, U., Ahmad, J., John, R.: Tensile creep and fatigue of Sylramic-iBN melt-infiltrated SiC matrix composites: Retained properties, damage development, and failure mechanisms. Compos. Sci. Tech. **68**, 3305–3313 (2008)
5. Evans, A.G., Zok, F.W.: Review: the Physics and mechanics of fiber-reinforced brittle matrix composites. J. Mater. Sci. **29**, 3857–3896 (1994)
6. Kerans, R.J., Parthasarathy, T.A.: Crack deflection in ceramic composites and fiber coating design criteria. Compos. A **30**, 521–524 (1999)

7. Kerans, R.J., Hay, R.S., Parthasarathy, T.A., Cinibulk, M.K.: Interface design for oxidation-resistant ceramic composites. J. Am. Ceram. Soc. **85**(11), 2599–2632 (2002)
8. Marshall, D., Evans, A.G.: Acta Metall **37**, 2567–2583 (1989)
9. Naslain, R.: Design, preparation and properties of non-oxide CMCs for application in engines and nuclear reactors: an overview. Compos. Sci. Tech. **64**, 155–170 (2004)
10. McNulty, J.C., He, M.Y., Zok, F.W.: Notch sensitivity of fatigue life in a Sylramic™/SiC composite at elevated temperature. Compos. Sci. Tech. **61**, 1331–1338 (2001)
11. Prewo, K.M., Batt, J.A.: The oxidative stability of carbon fibre reinforced glass-matrix composites. J. Mater. Sci. **23**, 523–527 (1988)
12. Mah, T., Hecht, N.L., McCullum, D.E., Hoenigman, J.R., Kim, H.M., Katz, A.P., Lipsitt, H.A.: Thermal stability of SiC fibres (Nicalon). J. Mater. Sci. **19**, 1191–1201 (1984)
13. Heredia, F.E., McNulty, J.C., Zok, F.W., Evans, A.G.: An oxidation embrittlement probe for ceramic matrix composites. J. Am. Ceram. Soc. **78**, 2097–2100 (1995)
14. More, K.L., Tortorelli, P.F., Ferber, M.K., Keiser, J.R.: Observations of accelerated silicon carbide recession by oxidation at high water-vapor pressures. J. Am. Ceram. Soc. **83**(1), 211–213 (2000)
15. More, K.L., Tortorelli, P.F., Ferber, M.K., Walker, L.R., Keiser, J.R., Brentnall, W.D., Miralya, N., Price, J.B.: Exposure of ceramic and ceramic-matrix composites in simulated and actual combustor environments. In: Proceedings of international gas turbine and aerospace congress. Paper No. 99-GT-292 (1999)
16. Ferber, M.K., Lin, H.T., Keiser, J.R.: Oxidation behavior of non-oxide ceramics in a high-pressure, high-temperature steam environment. In: Jenkins, M.G., Lara-Curzio, E., Gonczy, S.T. (eds) Mechanical, Thermal, and Environmental Testing and Performance of Ceramic Composites and Components. pp. 210–215. ASTM STP 1392, American Society for Testing and Materials, OH (2000)
17. Morscher, G.N., Pujar, V.V.: Creep and stress–strain behavior after creep for SiC fiber reinforced, melt-infiltrated SiC matrix composites. J. Am. Ceram. Soc. **89**(5), 1652–1658 (2006)
18. Ojard, G., Gowayed, Y., Chen J, Santhosh, U., Ahmad, J., Miller, R., John, R.: Time-dependent response of MI SiC/SiC composites part I: standard samples. Ceram. Eng. Sci. Proc. **28**(2), 145–154 (2007)
19. Ojard, G., Calomino, A., Morscher, G., Gowayed, Y., Santhosh, U., Ahmad, J., Miller, R., John, R.: Post creep/dwell fatigue testing of MI SiC/SiC composites. Ceram. Eng. Sci. Proc. **28**(2), 135–143 (2007)
20. DiCarlo, J.A., Yun, H.-M., Morscher, G.N., Bhatt, R.T.: SiC/SiC composites for 1200°C and above. In: Bansal, N. (ed.) Hand book of ceramic composites, pp. 77–98. Kluwer, NY (2005)
21. Lundberg, R., Pompe, R., Carlsson, R., Goursat, P.: Fibre reinforced silicon nitride composites. Compos. Sci. Tech. **37**, 165–176 (1990)
22. Sirieix, F., Goursat, P., Lemcote, A., Dauger, A.: Pyrolysis of polysilazanes: relationship between precursor architecture and ceramic microstructure. Compos. Sci. Tech. **37**, 7–19 (1990)
23. Gonon, M.F., Fantozzi, G., Murat, M., Disson, J.P.: Association of the CVI process and of the use of polysilazane precursor for the elaboration of ceramic matrix composites reinforced by continuous fibres. J. Eur. Ceram. Soc. **15**, 185–190 (1995)
24. Yun, H.M., Gyekenyesi, J.Z., Chen, Y.L., Wheeler, D.R., DiCarlo, J.A.: Tensile beahvior of SiC/SiC composites reinforced by treated Sylramic SiC fibers. Ceram. Eng. Sci. Proc. **22**(3), 521–531 (2001)